

# Electrodynamic models of 2D materials: can we match thin film and single sheet approach?

Bruno Majérus<sup>a</sup>, Evdokia Dremetsika<sup>b</sup>, Michaël Lobet<sup>a,c</sup>,  
 Luc Henrard<sup>a</sup>, Pascal Kockaert<sup>b</sup>

<sup>a</sup> Department of Physics & Research Group on Carbon Nanostructures (CARBONNAGE), University of Namur, 61 rue de Bruxelles, B-5000 Namur, Belgium.

<sup>b</sup> OPERA-photonics, Université libre de Bruxelles (U.L.B.), 50 Avenue F. D. Roosevelt, CP 194/5, B-1050 Bruxelles, Belgium

<sup>c</sup> John A. Paulson School of Engineering and Applied Sciences, Harvard University, 9 Oxford Street, Cambridge, MA 02138, United States of America

E-mail: [Pascal.Kockaert@ulb.ac.be](mailto:Pascal.Kockaert@ulb.ac.be)

**Abstract.** In the study of their electromagnetic response, 2D-materials can be modeled as single sheets with a surface susceptibility (or conductivity) or as thin films with an effective permittivity implying a certain thickness. Since 2D materials are intrinsically anisotropic, both models have to take into account out-of-plane components in their anisotropic permittivity tensors. We compare both approaches and show that the corresponding transfer matrices are equivalent in the limit of small induced phase shifts, both for TE and TM cases. Consequently, our approach enables direct analytical relations connecting the effective permittivity tensor components and the surface susceptibility ones. The range of validity of the small phase shift approximation is numerically tested. Furthermore, we apply our formalism in order to obtain analytical relations for three relevant experimental quantities: the transmittance, the ellipsometric data and the contrast ratio. Finally, we discussed how the anisotropy can explain similarities and discrepancies reported in literature when using either a thin film or a single sheet approach. This study is of prime necessity to accurately model electromagnetic interactions with 2D materials.

## 1. Introduction

The electromagnetic properties of 2D materials are at the forefront of the present research activities. Further developments for applications as diverse as optical modulators, transparent conductive films, photovoltaic systems, superabsorbers or sensors request an accurate description of the electromagnetic response of systems based on 2D materials [1, 2, 3, 4]. For example, optical contrast or transmission are among the commonly used quantities to characterize 2D systems. One can determine their thickness or their number of layers [5, 6, 7, 8, 9]. Furthermore, electromagnetic properties are the macroscopic fingerprints of elementary excitations such as the interband transition, excitons or plasmons. Therefore their correct analysis is crucial to the understanding of the underlying physics of 2D materials.

Several models have been recently used in this context. The electronic response to an external field has been first considered as a purely 2D phenomenon with the definition of a single sheet (surface) conductivity  $\sigma^s$ , or similarly with a susceptibility

$\chi^s$  [10, 11]. In particular, for graphene, an analytical expression for  $\sigma^s$  based on tight-binding approximation and Kubo formula has become popular [12]. Both contributions of inter-band and intra-band electronic transitions are clearly distinguished in those models. The surface conductivity can be determined experimentally, *e.g.* via Brewster angle measurements [13].

Using another approach, 2D materials have been considered as isotropic materials with a small but finite thickness [7, 8, 9, 14, 15]. This approach notably allows to use the well-developed transfer matrix technique to predict and interpret optical data (including ellipsometry) with widely available methodology and numerical codes. The thickness is often arbitrarily taken as the interlayer distance of the 3D counterpart of the 2D material [11, 16], considered as a fitting parameter [7] or evaluated based on the variation of the electronic density in the transverse direction [17]. However, these two approaches (a purely 2D surface conductivity and a 3D isotropic thin film) do not match as demonstrated analytically and numerically [18, 19] and give model-dependent interpretation for ellipsometry data [20]. This is particularly true for oblique incidence and TM (*p*-polarised) electromagnetic radiation [21]. Indeed, considering only a purely in-plane 2D conductivity means that the out-of-plane response of the layer is neglected while for an isotropic thin film, both the in-plane and out-of-plane response are linked. Very recently, a criteria has been proposed to determine in which condition the two models give similar results at normal incidence [22].

Anisotropic thin films have also been studied, and the out-of-plane component has been taken as a free parameter [20, 23, 24], as a non-responding component ( $\varepsilon_{zz} = 1$ ) or deduced from first principle approach calculations performed with periodic boundary conditions [25, 19]. Out-of-plane susceptibility of a purely 2D model has been recently considered by two of us for both linear and non-linear response of graphene [26]. The adequate description of the out-of-plane component is of prime necessity since very diverse 2D materials with potentially large out-of-plane polarisability compared to graphene are synthesized [27] or predicted [28].

In this work, we analyze analytically and numerically the conditions on the electromagnetic response function (surface susceptibility, dielectric tensor) and on the thickness of the effective thin film for a good comparison of the different approaches. In particular, we provide expressions that link the surface susceptibility of the single sheet to the ordinary and extraordinary optical constant of the equivalent thin film. We compare also the interpretation of the optical transmission, the ellipsometry and optical contrast measurements in order to determine the surface conductivity of the 2D materials.

## 2. Modelisation of 2D materials

In this section, we perform the comparison between the single sheet and the thin film approaches within the framework of transfer matrix formalism for stratified media [29, Sec. 4.6]. As a first step, we build the transfer matrix of a single sheet at the interface of two surrounding media (respectively *a* and *b*), as depicted on Fig. 1 (left). In a second step, we calculate the transfer matrix of a thin film with finite thickness ( $d_f$ ) (Fig. 1 right). We then analytically compare the two approaches and highlight the consequences on quantities that can be easily determined experimentally (transmittance, ellipsometric data, optical contrast).

Importantly, we insist here on the intrinsic anisotropy of 2D materials and its consequences on the modelisation. The single sheet is described by a surface

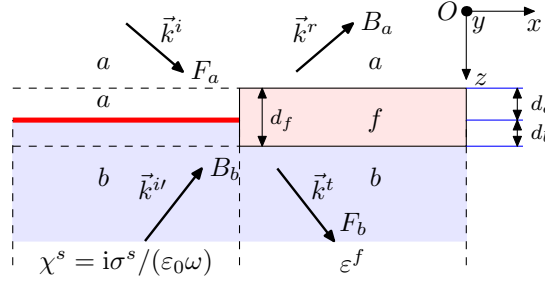


**Figure 1.** Schematic representation of the two studied configurations. Left: current sheet model; Right: thin film with an effective material  $f$  extending over a distance  $d_a$  (resp.  $d_b$ ) on the  $a$  (resp.  $b$ ) side. The reference frame is  $Oxyz$ , and the wave vectors are  $\vec{k}^i$  (incident wave),  $\vec{k}^r$  (reflected wave), and  $\vec{k}^t$  (transmitted wave). The forward and backward fields are denoted by  $F$  and  $B$ .

susceptibility tensor  $\chi^s$  diagonal in our basis vectors set (Fig. 1). The in-plane components of the 2D material are directly related to its surface conductivity by

$$\sigma_{ii}^s = -i\epsilon_0\omega\chi_{ii}^s \quad (1)$$

where  $ii = xx, yy$ . The out-of-plane component of the susceptibility,  $\chi_{zz}^s$ , is also considered but an out-of-plane conductivity has no physical meaning for a single sheet.

The thin film material is described by a dielectric tensor,  $\bar{\epsilon}^f$ , related to the bulk conductivity components by

$$\epsilon_i^f = \epsilon_0 + \frac{i\sigma_{ii}}{\omega}. \quad (2)$$

The in-plane and bulk conductivity are related by  $\sigma_{ii}^s = d_f \sigma_i$  [19]. The incident and substrate materials ( $a$  and  $b$ ) can be anisotropic but with their optical axes aligned with those of the 2D material, *i.e.*  $\epsilon_{ij}^{a,b} = \epsilon_0 \epsilon_i^{a,b} \delta_{ij}$ , which is the case in most (if not all) the systems studied experimentally so far. This hypothesis avoids the coupling between transverse electric (TE) and transverse magnetic (TM) modes. We allow those surrounding materials to have a complex permittivity, and express the dependence in the incident angle via the wavevector  $\vec{k} = (k_x, k_y, k_z)$ . If the incident medium is a perfect dielectric characterized by the real isotropic permittivity  $\epsilon_0 \epsilon_a = \epsilon_0 n_a^2$ , and  $k_y = 0$ , we have  $k_x = k_0 n_a \sin \alpha_i$ , with  $k_0$  the wavenumber of the light in vacuum and  $\alpha_i$  the incident angle.

### 2.1. 2D material as a single sheet

In order to describe the out-of-plane component in the single sheet model, we use the approach described in [26], based on [30, 31], as it allows to account for the out-of-plane component of the surface susceptibility. In particular, equations 5 and 6 of [26] provide expressions for the transmission coefficient of the electric field in TE and TM configurations, that can be written as

$$t = t_{ab} [1 + i(\varphi_x + \varphi_y + \varphi_z)], \quad (3)$$

$$r = t - 1 - 2i\varphi_x, \quad (4)$$

with the parameters defined in Table 1, where  $t_{ab}$  is the transmission coefficient in absence of the 2D material. We note that  $t_{ab}$  depends on the propagation direction

**Table 1.** Definition of the coefficients in TE and TM configuration, to the first order in  $\varphi_x, \varphi_y, \varphi_z$ . In these expressions,  $m$  and  $n$  will be replaced by  $a$ ,  $b$  and  $f$  to denote respectively the incidence medium, the substrate and the thin film.

	TE (s-polarization)	TM (p-polarization)
$t$	$E^t/E^i$	$D^t/D^i$
$r$	$E^r/E^i$	$D^r/D^i$
$k_0$		$\omega/c$
$k_x$		in-plane component of input $\vec{k}$
$k_z^m$	$\sqrt{\varepsilon_y^m k_0^2 - k_x^2}$	$\sqrt{\varepsilon_x^m (k_0^2 - k_x^2/\varepsilon_z^m)}$
$\alpha_{mn}$	$k_z^n/k_z^m$	$(\varepsilon_x^m k_z^n)/(\varepsilon_x^n k_z^m)$
$t_{mn}$		$2/(1 + \alpha_{mn})$
$r_{mn}$		$t_{mn} - 1$
$\varphi_x$	0	$\frac{k_z^a k_z^b}{\varepsilon_x^b k_z^a + \varepsilon_x^a k_z^b} \chi_{xx}^s$
$\varphi_y$	$\frac{k_0^2}{k_z^a + k_z^b} \chi_{yy}^s$	0
$\varphi_z$	0	$\frac{k_x^2}{\varepsilon_x^b k_z^a + \varepsilon_x^a k_z^b} \frac{\varepsilon_x^a \varepsilon_x^b}{\epsilon_{ab}} \chi_{zz}^s$
$\epsilon_{ab}$		$\frac{2}{(1/\varepsilon_z^a + 1/\varepsilon_z^b)}$
$\varphi_+$		$\varphi_x + \varphi_y + \varphi_z$
$\varphi_-$		$\varphi_x - \varphi_y - \varphi_z$
$\chi_{jj}^s$		$i\sigma_{jj}^s/(\varepsilon_0 \omega)$

and is therefore not symmetrical, *i.e.*  $t_{ba} = 2 - t_{ab}$ , while  $\varphi_x, \varphi_y, \varphi_z$  do not depend on the propagation direction.

In these notations the transfer matrix between the incident medium  $a$  and the outgoing medium (substrate)  $b$  can be written as

$$\mathcal{S}_{ab} = \frac{1}{t_{ab}} \cdot \begin{pmatrix} 1 - i\varphi_+ & r_{ab} + i\varphi_- \\ r_{ab} - i\varphi_- & 1 + i\varphi_+ \end{pmatrix}, \quad (5)$$

so that the forward ( $F$ ) and backward ( $B$ ) field components in media  $a$  and  $b$  at the single sheet interface are linked by

$$\begin{pmatrix} F_a \\ B_a \end{pmatrix} = \mathcal{S}_{ab} \begin{pmatrix} F_b \\ B_b \end{pmatrix}. \quad (6)$$

The expressions for TE and TM modes have a similar form if the fields appearing in (6) are the electric (resp. displacement) fields in the TE (resp. TM) configuration with coefficients defined as in Tab. 1.

The matrix  $\mathcal{S}_{ab}$  includes the out-of plane response of the current sheet  $\chi_{zz}$  through  $\varphi_z$ , and can therefore be compared to the thin film model.

## 2.2. 2D material as a thin film

We present in this section the propagation in the effective thin film system of thickness  $d_f$  described by the diagonal  $\bar{\varepsilon}^f$  of components  $\varepsilon_x^f$ ,  $\varepsilon_y^f$ , and  $\varepsilon_z^f$ . The total transfer matrices of the thin film ( $\mathcal{T}_{ab}$ ) involves the transfer matrix at the two interfaces ( $\mathcal{I}_{af}$  and  $\mathcal{I}_{fb}$ ) and the propagation matrix  $\mathcal{P}_f$  in the homogeneous film  $f$  over a distance  $d_f$ . Then

$$\mathcal{T}_{ab} = \mathcal{I}_{af} \mathcal{P}_f(d_f) \mathcal{I}_{fb} \quad (7)$$

with

$$\mathcal{P}_m(d_m) = \begin{pmatrix} e^{-i\Phi_m} & 0 \\ 0 & e^{i\Phi_m} \end{pmatrix}, \quad (8)$$

$$\mathcal{I}_{mn} = \frac{1}{t_{mn}} \begin{pmatrix} 1 & r_{mn} \\ r_{mn} & 1 \end{pmatrix}, \quad (9)$$

where  $\Phi_m = k_z^m d_m$ ,  $d_m$  is the thickness of layer  $m$ , and  $k_z^m$ ,  $r_{mn}$  and  $t_{mn}$  are defined in Tab. 1. The anisotropy of the media is described through the different components of the dielectric tensors.

### 2.3. Analytical comparison

The two models are considered equivalent if their transfer matrices are identical. However, we cannot directly compare  $\mathcal{S}_{ab}$  and  $\mathcal{T}_{ab}$  since the propagation in the slab of thickness  $d_f = d_a + d_b$  is not considered in  $\mathcal{S}_{ab}$ . The correct equality is then

$$\mathcal{T}_{ab} = \mathcal{P}_a(d_a) \mathcal{S}_{23} \mathcal{P}_b(d_b). \quad (10)$$

In the limit of small phase shift, we can develop to the first order in  $k_0 d_f$  for the bulk parameters ( $\Phi_a, \Phi_b, \Phi_f \ll 1$ ), and to the first order in  $k_0 \chi^s$  for the single sheet parameters ( $\varphi_x, \varphi_y, \varphi_z \ll 1$ ). From equation 10, a lengthy but straightforward calculation provides the effective dielectric function of the thin film as

$$\varepsilon_x^f = \chi_{xx}^s / d_f + \eta_a \varepsilon_x^a + \eta_b \varepsilon_x^b, \quad (11)$$

$$\varepsilon_y^f = \chi_{yy}^s / d_f + \eta_a \varepsilon_y^a + \eta_b \varepsilon_y^b, \quad (12)$$

$$\frac{1}{\varepsilon_z^f} = \frac{\eta_a}{\varepsilon_z^a} + \frac{\eta_b}{\varepsilon_z^b} - \frac{\chi_{zz}^s}{\epsilon_{ab} d_f}, \quad (13)$$

where  $\eta_a = d_a / d_f$ , and  $\eta_b = d_b / d_f$  and then  $\eta_a + \eta_b = 1$  (Fig. 1). As expected, the effective dielectric tensor components do not depend on the incident angle. Nevertheless, those quantities depend on the 2D material through  $\chi^s$  and on the geometry of the thin film defined by  $d_a$  and  $d_b$ . More surprisingly, the dielectric tensor of the two surrounding materials  $\bar{\varepsilon}^a$  and  $\bar{\varepsilon}^b$  also appears. In the frequent case where the incident medium is air, and the thin film of thickness  $d_f$  is lying on top of the substrate  $b$ , we have  $d_a = d_f$ ,  $d_b = 0$  and  $\varepsilon_i^a = 1$ , so that

$$\varepsilon_x^f = \chi_{xx}^s / d_f + 1, \quad (14)$$

$$\varepsilon_y^f = \chi_{yy}^s / d_f + 1, \quad (15)$$

$$\frac{1}{\varepsilon_z^f} = 1 + \frac{1 + \varepsilon_z^b}{2 \varepsilon_z^b d_f} \chi_{zz}^s. \quad (16)$$

Equations (14) and (15) are commonly used for 2D materials and demonstrate that (1) and (2) are perfectly valid under the assumptions reported above. The relation for the out-of-plane components (equations (13) and (16)) are far from being intuitive but are important to understand the link between the isotropic thin film and the anisotropic single sheet models. Indeed, they explain some discrepancies between the two approaches reported in the literature, as we will discuss later. Note that  $\chi_{zz}^s = 0$  gives  $\varepsilon_z^f = 1$ .

## 3. Discussion

In the following section we compare the results of our two approaches on quantities that are easily obtained experimentally: transmittance, ellipsometry and optical contrast.

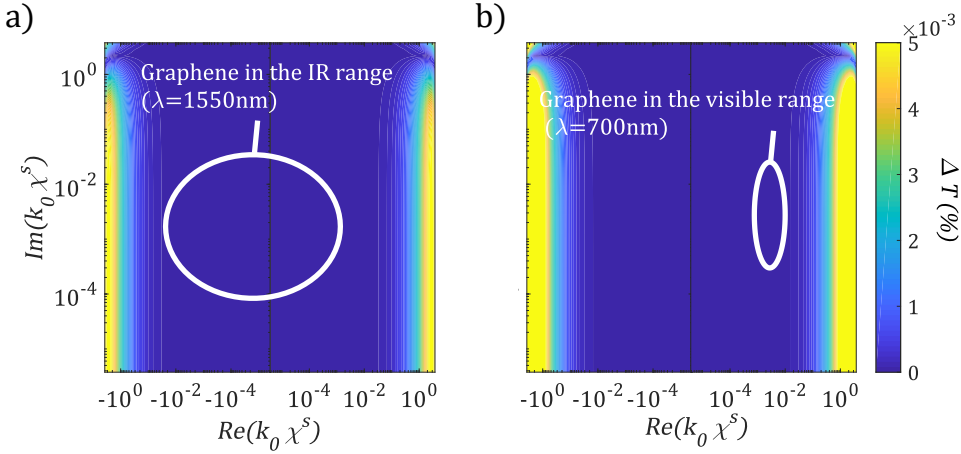


**Figure 2.** Relative difference  $\Delta T$  between the transmittance predicted by the single sheet and the thin film models, with respect to the real and imaginary part of  $k_0\chi^s$ . (a) Infrared wavelength ( $\lambda = 1550$  nm); (b) Visible wavelength ( $\lambda = 700$  nm). Circled areas indicate the range of values  $k_0\chi^s$  for graphene within the Kubo formula for a range of Fermi level from 0.05 eV to 1 eV and a range a relaxation time from 10 fs to 200 fs.

### 3.1. Transmittance

In TM configuration, from eq. 3 and table 1, the change in transmittance induced by the 2D material in the small phase shift hypothesis (first order in  $k_0d_f \equiv k_0\chi^s$ ) and for real  $\bar{\epsilon}_a$  and  $\bar{\epsilon}_b$  is

$$\left| \frac{t}{t_{ab}} \right|^2 - 1 = - t_{ab} \frac{k_z^b}{\varepsilon_z^b} \text{Im}\chi_{xx}^s \left[ 1 + \frac{k_x^2}{k_z^a k_z^b} \frac{\varepsilon_x^a \varepsilon_z^b}{\epsilon_{ab}} \left( \frac{\text{Im}\chi_{zz}^s}{\text{Im}\chi_{xx}^s} \right) \right] \quad (17)$$

$$= - t_{ab} \frac{k_z^b}{\varepsilon_z^b} \text{Im}\varepsilon_x^f d_f \left[ 1 + \frac{k_x^2}{k_z^a k_z^b} \frac{(\varepsilon_x^a)^2 \varepsilon_z^b}{|\varepsilon_z^f|^2} \left( \frac{\text{Im}\varepsilon_z^f}{\text{Im}\varepsilon_x^f} \right) \right]. \quad (18)$$

The change in transmittance (17) is only related to  $\text{Im}\chi^s$  and, via (1), to  $\text{Re}\sigma^s$ . Simple transmittance measurements can therefore provide no information about  $\text{Re}\chi^s$ , or  $\text{Im}\sigma^s$ . In contrast, (18) depends also on  $\text{Re}\varepsilon_z^f$  through  $|\varepsilon_z^f|^2$ .

To understand the impact of using the thin film model instead of the single sheet approach, and to test the validity range of (11)–(13) with respect to  $k_0\chi^s$ , we have performed extensive numerical simulations. All our results are for a TM wave incident on an air/2D/fused quartz system with an angle  $\theta = 75^\circ$ , and a thickness  $d_f = 0.34$  nm, except otherwise specified.

Fig. 2 shows the difference of transmittance ( $\Delta T$ ) for two incident wavelengths (1550 nm and 700 nm) obtained with the single sheet model with no out-of-plane susceptibility ( $\chi_{zz}^s = 0$ ) and with the anisotropic thin film with  $\bar{\epsilon}^f$  from (11)–(13).

Within the small phase shift condition, the transmittance predicted by the *anisotropic* thin film model and the single sheet model are obviously in very good agreement. When the small phase shift condition is relaxed ( $\text{Re}[k_0\chi^s] \gtrsim 1$ ), a small discrepancy can be observed, especially when  $k_0$  increases [See Fig 2(b)]. For a better

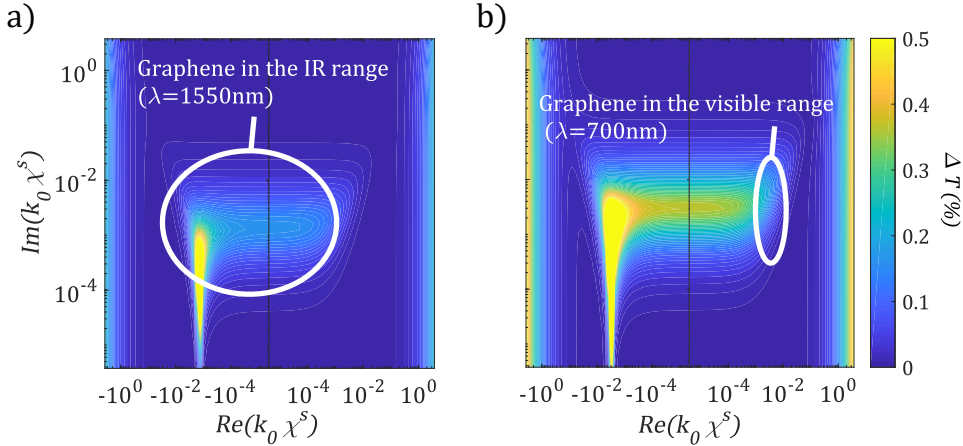


**Figure 3.** Same as Fig. 2 for the isotropic thin film model

interpretation of the data, we identify on the figure possible values for graphene conductivity based on the Kubo formula, which depends strongly on the Fermi level and the scattering mean time of the electrons. For this particular case of graphene, we observe a particularly small  $\Delta T$ . Maximum discrepancy between the two models is  $5 \cdot 10^{-3}\%$ . Therefore, in the following, we will consider that the single sheet model and the anisotropic thin film model give equivalent results.

Interestingly, an isotropic thin film model shows more important discrepancies, as illustrated on Fig. 3. Note that the scale of  $\Delta T$  is different on Fig. 2 and Fig. 3. In this case,  $\varepsilon_x$  and  $\varepsilon_y$  are equal and obtained from (11) and (12) and  $\varepsilon_x = \varepsilon_y = \varepsilon_z$ . For a large range of values, isotropic and anisotropic thin film models provide almost the same results.

However, a high value of  $\Delta T$  is observed on a vertical line corresponding to  $\text{Re}[\chi^s] = d_f$ , for which the real part of the permittivity  $\varepsilon = 1 - \chi^s/d_f$  vanishes. This shows, similarly to what was reported in [21], that an artificial plasmonic resonance is predicted by an *isotropic* thin film model, due to the artificial metallic nature of the out-of-plane component of the permittivity tensor. This unphysical resonance could have dramatic effects on the prediction of the optical properties.

To investigate further the influence of the anisotropy, we present the difference between the transmittance obtained with the isotropic and anisotropic thin film models in TM configuration for graphene, with respect to the incident wavelength (Fig. 4). The two models give very similar results for a ratio  $\lambda/d_f > 1000$  (dashed line) (*i.e.* very small  $k_0 d_f$ ) with  $\theta = 75^\circ$ . Obviously, close to normal incidence the models match even better. This validates the fact that the anisotropy of graphene has been often disregarded without consequences on the validity of the conclusions.

The surprising good prediction within the isotropic thin film model for intrinsically anisotropic 2D material could be explained. Indeed the isotropic thin film model does not correspond to the assumption  $\chi_{zz}^s = \chi_{xx}^s$ , but to  $\varepsilon_z^f = \varepsilon_x^f$ . By means of (13), this is equivalent to set

$$\text{Im}\chi_{zz}^s = \frac{\varepsilon_x^a \varepsilon_{ab}}{|\varepsilon_z^f|^2} d_f \text{Im}\varepsilon_z^f = \frac{\varepsilon_x^a \varepsilon_{ab}}{|1 + \chi_{xx}^s/d_f|^2} \text{Im}\chi_{xx}^s, \quad (19)$$

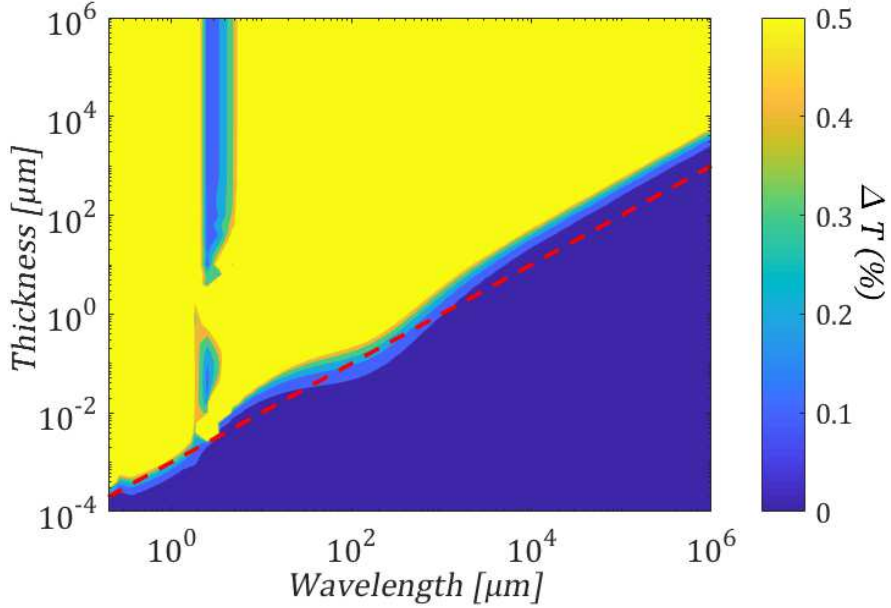


**Figure 4.** Difference of graphene transmittance  $\Delta T$  between the isotropic and anisotropic thin film. Fermi level  $E_F = 0.4$  eV and relaxation time  $\tau = 100$  fs. The red dotted line represent a thickness equal to 1/1000 of the wavelength.

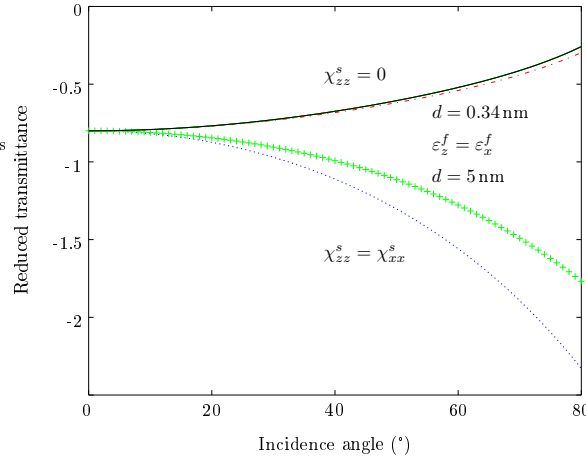


**Figure 5.** Reduced transmittance [brackets in (17) and (18)] for and air/graphene/glass structure:  $n_a = 1$ ,  $n_b = 1.5$ ,  $\chi_{xx}^s = (1.50 + 2.29i)$  nm at a wavelength of 634 nm [15]. Curves are for: anisotropic single sheet with no out-of-plane response ( $\chi_{zz}^s = 0$ ) (—) ; isotropic thin film model ( $\varepsilon_z^f = \varepsilon_x^f$ ) with  $d_f = 0.34$  nm (—) and  $d_f = 5$  nm (—) ; isotropic current sheet model ( $\chi_{zz}^s = \chi_{xx}^s$ ) (—).

which shows that the isotropic thin film model tends to the *anisotropic* single sheet one with  $\chi_{zz}^s = 0$  when  $|\chi_{xx}^s|^2 \gg d_f^2$ , as in this case eq. (19) provides  $\chi_{zz}^s \approx 0$ .

This justifies that the isotropic thin film model can be used with good results to model graphene with  $\text{Im}[\chi_{zz}^s] = 0$ , and  $d_f = 0.34 \text{ nm}$ . In particular, it confirms that in the limit  $d_f = 0$ , both models agree, as reported in [32]. More importantly, this also resolves the apparent contradiction between the conclusions of [32], and those of [19, 18, 21] on the equivalence (or not) of both models for  $d_f \rightarrow 0$ . Indeed, (19) shows that if we model graphene by means of a thicker layer so that  $\chi_{xx}^s \ll d_f \ll 1/k_0$ , the isotropic thin film model would correspond to the *isotropic* single sheet one ( $\chi_{xx}^s = \chi_{zz}^s$ ) in the particular case were  $n_a = n_b = 1$  and no more to the *anisotropic* single sheet with  $\chi_{zz}^s = 0$ . We illustrate this analytical observation on Fig. 5, where we plot the bracket in (17) and (18) for an air/graphene/glass system at 634 nm as function of the incident angle for different modelisations of the same system: the single sheet for  $\chi_{zz}^s = 0$  (full line) and with ( $\chi_{xx}^s = \chi_{zz}^s$ ) (dashed line), the isotropic thin film for  $d_f = 0.34 \text{ nm}$  (dot-dashed line) and  $d_f = 5 \text{ nm}$  (crosses). Once again, the results for the anisotropic thin film cannot be distinguished from those of the anisotropic single sheet. The last value of  $d_f$  is commonly used in discrete numerical simulations to avoid prohibitive numerical cost [21]. As the anisotropy does not play any role at normal incidence, all the curves are superimposed. As the angle of incidence increases, the  $z$  component of the response functions becomes more important and the precise value of the thickness of the thin film influences the computed optical properties.

Although transmittance change at different angles would in principle allow to separate the in-plane and the out-of-plane responses of the imaginary part of the susceptibility (real part of the conductivity), these measurements are usually performed at normal incidence, for which the TE and TM cases coincide.

### 3.2. Ellipsometry

Ellipsometry records the ratio of the reflexion or transmission of a sample in TM and TE configurations, at different angles. From equations (3) and (4), in the small phase approximation (*i.e.* to the first order in  $k_0 \chi^s$ ), we get

$$\rho_t = \frac{t^{TM}}{t^{TE}} = \frac{t_{ab}^{TE}}{t_{ab}^{TM}} [1 + i(\varphi_x^{TM} - \varphi_y^{TE} + \varphi_z^{TM})]. \quad (20)$$

Under the assumption that  $\chi_{xx}^s = \chi_{yy}^s$ , using Tab. 1, we can write

$$\rho_t \frac{t_{ab}^{TM}}{t_{ab}^{TE}} - 1 = -\frac{ik_x^2}{k_z^a + k_z^b} \left( \chi_{xx}^s - \frac{\varepsilon_x^a \varepsilon_x^b}{\epsilon_{ab}} \chi_{zz}^s \right). \quad (21)$$

The in-plane  $\chi_{xx}^s$  and the out-of plane  $\chi_{zz}^s$  susceptibilities can then not be separated by means of standard transmission ellipsometry because the ratio between the out-of-plane and the in-plane susceptibilities is independent of  $k_x$  and  $k_z$ , and therefore of the incidence angle.

Let define the parenthesis in (21) as

$$\chi^{ell} = \chi_{xx}^s - \frac{\varepsilon_x^a \varepsilon_x^b}{\epsilon_{ab}} \chi_{zz}^s. \quad (22)$$

We can now provide a simple explanation to the difference reported in [20] between the permittivity extracted from ellipsometric data using the thin film and the single sheet models for MoS<sub>2</sub>. In the following, we named  $[\chi_{xx}^s]_i$  (resp.  $[\chi_{xx}^s]_a$ ) the in-plane susceptibility obtained with the isotropic thin film (resp. anisotropic single sheet) model. In figure 6, we reproduce results published in [20].

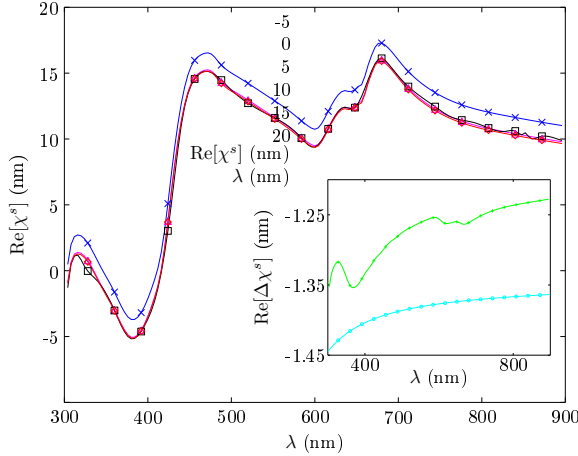


**Figure 6.** Values of  $\text{Re}\chi^s$  for MoS<sub>2</sub> single layer retrieved using different models: (x) isotropic thin film model from [20]; (□) anisotropic current sheet model from [20]; (o) calculated from (x) using the shift calculated from (24) (+ in the inset); (△) is (x) shifted by  $-\varepsilon_x^b d$  (o in the inset). Sellmeier's equation provided by Schott for its N-BK7 is used to calculate  $\varepsilon_b$ .

The highest curve (x) is obtained by fitting the ellipsometric data with an isotropic thin film model. This is equivalent to assume  $\varepsilon_z^f = \varepsilon_x^f$ , or using (16),  $\chi_{zz}/\epsilon_{ab} = \chi_{xx}/\varepsilon_x^f$ , so that

$$\chi^{ell} = [\chi_{xx}^s]_i \left( 1 - \frac{\varepsilon_x^b}{1 + [\chi_{xx}^s]_i/d_f} \right). \quad (23)$$

The other curves correspond to the anisotropic single sheet model with  $\chi^{ell} = [\chi_{xx}^s]_a$ . The deduced in-plane single sheet susceptibilities can be compared and

$$[\chi_{xx}^s]_a = [\chi_{xx}^s]_i - \varepsilon_x^b d_f + \frac{\varepsilon_x^b d_f}{1 + [\chi_{xx}^s]_i/d_f}, \quad (24)$$

in which the last term is negligible for MoS<sub>2</sub> in the wavelength range under consideration. This is verified directly on Fig. 6, where the curve obtained by means of the isotropic thin film model has been shifted by an amount  $-\varepsilon_x^b d_f$ , with  $d_f = 0.615$  nm, and  $\varepsilon_x^b$  for BK7 (substrate). This provides an excellent agreement with the anisotropic model. We do not reproduce the imaginary part of the susceptibility (real part of the conductivity), as it is not affected by the real shift  $-\varepsilon_x^b d_f$ , as was shown in [20].

This good agreement between experimental data and our analytical predictions again confirms the validity of the small phase shift approximation ( $k_0\chi^s \ll 1$ ).

We conclude that standard ellipsometry provides no information on the  $x - z$  anisotropy of the 2D sample. However, without the formalism presented in Sec. 2.1, the single sheet approach imposes implicitly  $\chi_{zz}^s = 0$ , while the isotropic thin film approach assumes  $\chi_{zz}^s = \epsilon_{ab}\chi_{xx}^s/\varepsilon_x^f$ , which explains differences reported in the literature, for the retrieval of  $\chi_{xx}^s$  from ellipsometric data. Equation (22) allows to introduce in the fitting procedure of these data a value for  $\chi_{zz}^s$  based on theoretical assumptions or obtained experimentally, for example, by means of contrast ratio measurements.

### 3.3. Contrast ratio

The contrast ratio of 2D materials on a thick substrate is often very small and hardly measurable. However, reflexion microscopy and contrast ratio are commonly used to determine the presence of graphene (or the number of layers) if a thin dielectric film is lying on the top of the substrate, most often  $\text{SiO}_2$  on Si [33, 6, 5]. This additional layer creates interferences that depend on the graphene susceptibility and allows to tune the total reflectance of the system, by choosing the layer composition and its thickness. Measurements are usually performed at normal incidence, so that only the in-plane susceptibility is probed. To take into account the additional layer, we should multiply  $\mathcal{T}_{ab}$  in (10) by a propagation matrix accounting for the propagation in the additional layer, and an interface matrix between this layer and the substrate. As the matrix  $\mathcal{T}_{ab}$  is the same in the current sheet and thin film approaches, the final result do not depend on the chosen model, especially at normal incidence for which the isotropic and anisotropic thin film models are equivalent.

The contrast ratio depends on the real part of the in-plane susceptibility of the 2D material. However, this measurement is strongly dependent on the parameters of the top layer, including their thickness and permittivity. This explains probably the differences in fitting experimental data that were reported in [18].

## 4. Conclusions

We have explored analytically and numerically the link between the modeling of a 2D material by means of a current sheet or thin film model. We have focused our analysis on the description of the intrinsic anisotropy of the layers, *i.e.* the effect of the out-of-plane component of the single sheet or the out-of-plane component of the dielectric tensor of the thin film. The analytical equivalence of the anisotropic thin film and the current sheet models in the small phase shift condition shows that most discrepancies between these two approaches do not come from the finite thickness of the thin film, but from an incorrect description of the anisotropy, mainly for TM polarization and oblique incidence. In particular, we have shown that assuming an isotropic dielectric function of a thin film is not equivalent to assume an isotropic single sheet susceptibility. We have also commented the fact that a single sheet with vanishing out-of-plane response (as graphene) corresponds to an isotropic or an anisotropic effective thin film depending of the considered thickness of the film.

The application of the transfer matrix approach to classical measurement schemes provide evidence that a combination between different techniques is needed to characterize an in-plane isotropic material, as

- transmittance change for a 2D material on dielectric provides  $\text{Im}[\chi_{xx}]$  at normal incidence and could provide  $\text{Im}[\chi_{zz}]$  at other incidence angle;
- standard ellipsometry, in transmission or reflexion, cannot separate the in-plane and out-of-plane contributions. However, combined with transmittance changes it could provide  $\text{Im}[\chi_{zz}^s]$ . Another way to retrieve  $\chi_{xx}^s$  and  $\chi_{zz}^s$  separately would be to perform ellipsometry experiments on different substrates;
- contrast ratio on a multilayer substrate combined with the previous methods can also provide information about  $\text{Re}[\chi_{xx}]$ , or even  $\text{Re}[\chi_{zz}]$  at oblique incidence.

We hope that the present single sheet transfer matrix approach, and the natural connection between its parameters and those of a thin film will help to perform the

analysis of stratified media involving 2D materials, either for the characterization of 2D materials, or for their use in various applications.

## Acknowledgments

Part of this research was performed while E. D. was funded by the Fund for Research Training in Industry and Agriculture (FRIA, Belgium), and M. L. was a recipient of a Fellowship of the Belgian American Educational Foundation.

## References

- [1] Yu S, Wu X, Wang Y, Guo X and Tong L *Advanced Materials* **29** 1606128 (*Preprint* <https://onlinelibrary.wiley.com/doi/pdf/10.1002/adma.201606128>) URL <https://onlinelibrary.wiley.com/doi/abs/10.1002/adma.201606128>
- [2] Bonaccorso F, Sun Z, Hasan T and Ferrari A C 2010 *Nature Photonics* **4** 611–622 ISSN 1749-4893 URL <https://www.nature.com/articles/nphoton.2010.186>
- [3] Ferrari A C, Bonaccorso F, Fal'ko V, Novoselov K S, Roche S, Boggild P, Borini S, Koppens F H L, Palermo V, Pugno N, Garrido J A, Sordan R, Bianco A, Ballerini L, Prato M, Lidorikis E, Kivioja J, Marinelli C, Ryhanen T, Morpurgo A, Coleman J N, Nicolosi V, Colombo L, Fert A, Garcia-Hernandez M, Bachtold A, Schneider G F, Guinea F, Dekker C, Barbone M, Sun Z, Galiotis C, Grigorenko A N, Konstantatos G, Kis A, Katsnelson M, Vandersypen L, Loiseau A, Morandi V, Neumaier D, Treossi E, Pellegrini V, Polini M, Tredicucci A, Williams G M, Hee Hong B, Ahn J H, Min Kim J, Zirath H, van Wees B J, van der Zant H, Occhipinti L, Di Matteo A, Kinloch I A, Seyller T, Quesnel E, Feng X, Teo K, Rupesinghe N, Hakonen P, Neil S R T, Tannock Q, Lofwander T and Kinaret J 2015 *Nanoscale* **7**(11) 4598–4810 URL <http://dx.doi.org/10.1039/C4NR01600A>
- [4] Mak K F and Shan J 2016 *Nature Photonics* **10** 216–226 ISSN 1749-4893 URL <https://www.nature.com/articles/nphoton.2015.282>
- [5] Bayle M, Reckinger N, Felten A, Landois P, Lancrey O, Dutertre B, Colomer J F, Zahab A A, Henrard L, Sauvajol J L and Paillet M *Journal of Raman Spectroscopy* **49** 36–45 (*Preprint* <https://onlinelibrary.wiley.com/doi/pdf/10.1002/jrs.5279>) URL <https://onlinelibrary.wiley.com/doi/abs/10.1002/jrs.5279>
- [6] Abergel D S L, Russell A and Fal'ko V I 2007 *Applied Physics Letters* **91** 063125 (*Preprint* <https://doi.org/10.1063/1.2768625>) URL <https://doi.org/10.1063/1.2768625>
- [7] Eichfeld S M, Eichfeld C M, Lin Y C, Hossain L and Robinson J A 2014 *APL Materials* **2** 092508 (*Preprint* <https://doi.org/10.1063/1.4893961>) URL <https://doi.org/10.1063/1.4893961>
- [8] Li H, Wu J, Huang X, Lu G, Yang J, Lu X, Xiong Q and Zhang H 2013 *ACS Nano* **7** 10344–10353 pMID: 24131442 (*Preprint* <https://doi.org/10.1021/nn4047474>) URL <https://doi.org/10.1021/nn4047474>
- [9] Ottaviano L, Palleschi S, Perrozzi F, D'Olimpio G, Priante F, Donarelli M, Benassi P, Nardone M, M Gonchigsuren, Gombosuren M, Lucia A, Moccia G and Cacioppo O A 2017 *2D Materials* **4** 045013 ISSN 2053-1583 URL <http://stacks.iop.org/2053-1583/4/i=4/a=045013>
- [10] Stauber T, Peres N M R and Geim A K 2008 *Phys. Rev. B* **78**(8) 085432 URL <https://link.aps.org/doi/10.1103/PhysRevB.78.085432>
- [11] Lobet M, Majerus B, Henrard L and Lambin P 2016 *Phys. Rev. B* **93**(23) 235424 URL <https://link.aps.org/doi/10.1103/PhysRevB.93.235424>
- [12] Falkovsky L A 2008 *Journal of Physics: Conference Series* **129** 012004 ISSN 1742-6596 URL <http://stacks.iop.org/1742-6596/129/i=1/a=012004>
- [13] Majerus B, Cormann M, Reckinger N, Paillet M, Henrard L, Lambin P and Lobet M 2018 *2D Materials* **5** 025007 URL <http://stacks.iop.org/2053-1583/5/i=2/a=025007>
- [14] Nelson F J, Kamineni V K, Zhang T, Comfort E S, Lee J U and Diebold A C 2010 *Applied Physics Letters* **97** 253110 (*Preprint* <https://doi.org/10.1063/1.3525940>) URL <https://doi.org/10.1063/1.3525940>
- [15] Cheon S, Kihm K D, Kim H g, Lim G, Park J S and Lee J S 2014 *Scientific Reports* **4** 6364 ISSN 2045-2322 URL <https://www.nature.com/articles/srep06364>
- [16] Lu J P 1997 *Phys. Rev. Lett.* **79**(7) 1297–1300 URL <https://link.aps.org/doi/10.1103/PhysRevLett.79.1297>
- [17] Wagner P, Ivanovskaya V V, Rayson M J, Briddon P R and Ewels C P 2013 *Journal of Physics: Condensed Matter* **25** 155302 URL <http://stacks.iop.org/0953-8984/25/i=15/a=155302>

- [18] Merano M 2016 *Phys. Rev. A* **93**(1) 013832 URL <https://link.aps.org/doi/10.1103/PhysRevA.93.013832>
- [19] Matthes L, Pulci O and Bechstedt F 2016 *Phys. Rev. B* **94**(20) 205408 URL <https://link.aps.org/doi/10.1103/PhysRevB.94.205408>
- [20] Jayaswal G, Dai Z, Zhang X, Bagnarol M, Martucci A and Merano M 2018 *Opt. Lett.* **43** 703–706 URL <http://ol.osa.org/abstract.cfm?URI=ol-43-4-703>
- [21] Valuev I, Belousov S, Bogdanova M, Kotov O and Lozovik Y 2016 *Applied Physics A* **123** 60 ISSN 1432-0630 URL <https://doi.org/10.1007/s00339-016-0635-1>
- [22] Li Y and Heinz T F 2018 *2D Materials* **5** 025021 URL <http://stacks.iop.org/2053-1583/5/i=2/a=025021>
- [23] Funke S, Miller B, Parzinger E, Thiesen P, Holleitner A W and Wurster U 2016 *Journal of Physics: Condensed Matter* **28** 385301 URL <http://stacks.iop.org/0953-8984/28/i=38/a=385301>
- [24] Kravets V G, Grigorenko A N, Nair R R, Blake P, Anissimova S, Novoselov K S and Geim A K 2010 *Phys. Rev. B* **81**(15) 155413 URL <https://link.aps.org/doi/10.1103/PhysRevB.81.155413>
- [25] Marinopoulos A G, Reining L, Rubio A and Olevano V 2004 *Phys. Rev. B* **69**(24) 245419 URL <https://link.aps.org/doi/10.1103/PhysRevB.69.245419>
- [26] Dremetsika E and Kockaert P 2017 *Phys. Rev. B* **96**(23) 235422 URL <https://link.aps.org/doi/10.1103/PhysRevB.96.235422>
- [27] Novoselov K S, Mishchenko A, Carvalho A and Castro Neto A H 2016 *Science* **353** ISSN 0036-8075 (Preprint <http://science.sciencemag.org/content/353/6298/aac9439.full.pdf>) URL <http://science.sciencemag.org/content/353/6298/aac9439>
- [28] Rasmussen F A and Thygesen K S 2015 *The Journal of Physical Chemistry C* **119** 13169–13183 (Preprint <https://doi.org/10.1021/acs.jpcc.5b02950>) URL <https://doi.org/10.1021/acs.jpcc.5b02950>
- [29] Azzam R M A 1987 *Ellipsometry and polarized light* (Amsterdam New York: North-Holland Sole distributors for the USA and Canada, Elsevier Science Pub. Co) ISBN 0-444-87016-4
- [30] Sipe J E 1987 *J. Opt. Soc. Am. B, JOSAB* **4** 481–489 ISSN 1520-8540 URL <https://www.osapublishing.org/abstract.cfm?uri=josab-4-4-481>
- [31] Felderhof B U and Marowsky G 1987 *Appl. Phys. B* **44** 11–17 ISSN 0946-2171, 1432-0649 URL <https://link.springer.com/article/10.1007/BF00693978>
- [32] Depine R A 2016 *Graphene Optics: Electromagnetic Solution of Canonical Problems* 2053-2571 (Morgan & Claypool Publishers) ISBN 978-1-6817-4309-7 URL <http://dx.doi.org/10.1088/978-1-6817-4309-7>
- [33] Blake P, Hill E W, Castro Neto A H, Novoselov K S, Jiang D, Yang R, Booth T J and Geim A K 2007 *Applied Physics Letters* **91** 063124 (Preprint <https://doi.org/10.1063/1.2768624>) URL <https://doi.org/10.1063/1.2768624>